Engineering and Technology Journal
Journal homepage: https://etj.uotechnology.edu.iq

Structural Characterization of ($Mg_{(1-x)}pb_xO$)-NPs by Modified Pechini Method

Israa A. Najem[a*], **Fadhil Abd Rasin**[b], **Shaker J. Edrees**[c]

[a,b] Materials Engineering Department., University of Technology-Iraq, Alsina'a Street, 10066 Baghdad, Iraq.
[c] College of Materials Engineering, University of Babylon-Iraq, Babylon, Iraq
*Corresponding author Email: israadnan2000@gmail.com.

HIGHLIGHTS

- The structure revealed that all the specimens have identical space groups and index well to a cubic structure.
- Crystallite size was increased with increasing the fraction of doping except for (Mg0.97Pb0.03O) due to the formation of PbO oxide.
- The molecular vibration of the pure and doped specimens has the same framework.
- As the incorporation of Pb^{2}+ ions increased, the bands got broader, and the intensities increased in the range of 800-400 cm^{-1} .

ARTICLE INFO

Handling editor: Jawad K. Oleiwi

Keywords: MgO-NPs; doping; PbO; Pechini; DTA; XRD; FTIR.

ABSTRACT

The structural characterization was discussed in the present paper of the pure MgO nanoparticles and the doped (Mg(1-x)pbxO) nanoparticles specimens, where ($0 \leq x \leq 0.03$). The modified Pechini method was used to prepare all the specimens. From (DTA), the convenient temperature of decomposition from Mg(OH)2 to MgO was above 375°C. The structure investigation (XRD) revealed that all the specimens have identical space groups and index well to cubic structures. The obtained crystallite size by Scherrer's equation was increased with increasing the fraction of doping except for (Mg0.97Pb0.03O) due to the formation of PbO oxide. The molecular vibration by FTIR demonstrated that all the pure and doped specimens have the same framework. As the incorporation of Pb2+ ions increases, the bands get broader, and the intensities increase in the ranging 800-400 cm-1 due to vibrations of O-Mg and O-Pb bands, respectively.

1. Introduction

The research on nanoparticles (NPs) shows novel properties dissimilar to bulk materials. The unique properties and the efficient performance of nanomaterials are determined by their surface structure, size, and particle interaction [1, 2]. The materials with nano-size possess a high proportion of surface area to Volume than their traditional structures, which can be prompted extra notable effect on their quality and synthetic reactivity [3]. The role that plays by the size of particles is similar, in some situations, to the chemical compositions of particles, by adding one more variable for designing and developing their behavior [2]. The nano-size materials have a promising development in many technological applications, including magnetic [4], bio [5], and fuel cells [6], and may ultimately be based on tailoring their behavior by adding impurities through doping.

Metal oxides nanoparticles were fields of nanoparticles (NPs) that could be utilized directly in applying popular chemical processes, with different magnetic and electronic characteristics that enable them to be utilized in particular places [7]. For instance of metal oxides nanoparticles TiO2-NPs [8], ZnO-NPs [9], Fe2O3-NPs [10] and MgO-NPs [11].

The magnesium oxide nanoparticles, with the sodium-chloride arrangement, have drawn the interest of many academics among these oxides owing to unusually functional materials commonly used in superconductors [12], antibacterial materials [13], and magnetic [14]. The properties of magnesia may ultimately depend on the progress of their behavior by doping.

Therefore, it is motivating from a technological viewpoint to dope magnesium oxide for a different types of ions besides the rare earth oxides to view the chance of the existence of magnetic and optical properties [15], which is a remarkable mechanism for the modification [16]. Dopants in nanocrystals lead to phenomena not found in the bulk because their electronic states are confined to a small Volume [17]. However, the dopant impurities have tuned the properties of metal oxide

http://doi.org/10.30684/etj.v40i6.2147
Received 28 April 2021; Accepted 20 June 2021; Available online 9 May 2022
2412-0758/University of Technology-Iraq, Baghdad, Iraq

nanoparticles in MgO [18-20]. Therefore, these dopants can be altered the properties, as in demand for their industrial requests as a magnetic sensor, optical, switching device, and as diluted magnetic semiconductor [18, 21], by modifying the energy gap [22, 23], the magnetic properties [24, 25], the antibacterial effect [26], the optical [24, 27], the conduction [28] and the Photoluminescence [29] properties.

The pure MgO-NPs and doped specimens were prepared via various routes, such as microwave. sol-gel [30], liquid-.phase [31], co-.precipitation [32], combustion [33], green synthesis [34], hard templating pathway [35], aerogel route [36], spinning disk reactor [37] sol-gel [26] and modification Pechini method [38]. The method of Pechini was selected as a favorite one due to its remarkable preparation of high-temperature superconductors, catalysts, and ceramics, magnetic materials [39]. The advantage of this method includes good control of particle morphology and good homogeneity [40].

Thus in the present work, the Pechini method was used to synthesize undoped MgO-NPs and doped (Mg(1.-x)pbxO)-NPs specimens ($0 \leq x \leq 0.03$). Furthermore, this paper explores the effect of incorporating different concentrations of Pb2+ ions into the structure of MgO-NPs host lattice, which was investigated by employing X-Ray Diffraction (XRD) and the Fourier Transition Infrared Spectra (FTIR). Also, the appropriate temperature of calcinated by thermally stability and decomposing behavior of Mg(OH)2 into MgO was investigated by thermal differential analysis DTA.

2. Experimental Method

2.1 Chemical Used

The Pb(NO3)2, lead nitrate (purity > 99%, chemicals PVT, India), Mg(NO3)2.6H2O, magnesium nitrate hexahydrate (purity > 99%, BDH chemicals Ltd, England), C6H8O7.H2O, citric acid (purity > 99%, CDH, India,), C2H6.O2 ,Ethylene glycol, EG, (chemicals PVT. LTD, India, purity > 99%) were used without any further purifications with distilled water to prepare (Mg(1.-x)pbxO) - NPs specimens, where ($0 \leq x \leq 0.03$) by using sol gel-modified Pechini method.

2.2 Preparation of specimens

The first stage of production is pure MgO-.NPs inVolved the creation of a stable aqueous solution, starting with citric acid solution and magnesium nitrate solution. They were dissolved in distilled water (100 ml) separately and stirred for 1 hour under constant stirring in these two separated solutions. The second stage inVolved chelating Mg2+ ions in the solution by mixing the citric acid solution with magnesium nitrate solution. However, the temperature of the mixed solutions was kept within a boundary of 90° C for 3 h. under fixed stirring. The third stage can be inVolved adding EG to control crystal growth, with a mass ratio of EG/ CA = 3/2. After some time, the color of the final solution began to change due to water evaporation to yellowish. The Final stage represents the formation of a totally viscous gel with a brown color. Then dehydrated, the obtained gel and calcinated in a furnace device (PIF 160/15- Made in Turkey) at a moderate temperature for 120 minutes at 420° C with a rate of heating 3°C./min. To preparation of (Mg(1-x)pbxO)-NPs doped specimen, where ($0 \leq x \leq 0.03$). This involves the preparation of an additional stabilized hydrous solution of lead nitrite that was dissolved in the distilled water individually and stirred for 1 h. Then, the citric acid is added into a mixture of lead nitrite and magnesium nitrite to chelate Pb2+ and Mg2+ in the solution. Continued same procedures to produce all the (Mg(1-x)pbxO)-NPs powder specimens.

3. Instrumentals Techniques

All the pure and doped (Mg(1-x)PbxO)-NPs specimens, where ($0 \leq x \leq 0.03$), were tested by the powder of obtained specimens. The structure of the produced specimens was analyzed by employing X-Ray Diffraction using a diffractometer (Shimadzu-6000 with Cu-Kα beam λCu=1.5406Å) and Fourier transform infrared spectroscopy FTIR spectroscopy device (lapX\ Canada). Differential thermal analysis. (DTA-50 Shimadzu Japan) was used to investigate the temperature of calcinated.

4. Results and Discussion

4.1 Thermal Differential Analysis DTA

To examine the thermal stability and oxidation behavior of $Mg(OH)_2$ into MgO and detect a convenient calcination temperature for constructing MgO powder. The obtained precursor of pure Mg(OH)2 sample was subjected to DTA analysis by heating the untreated specimen in the temperature area from 25.-800 °C at a rate of $10°.C\backslash.min^{-1}$.

Figure 1 DTA graph of $Mg(OH)_2$ attained by the reaction of magnesium nitrite with citric acid. It is found from the (DTA) curve that the prepared $Mg(OH)_2$ decomposition thermally by experiencing three thermal stages. The first one is related to the elimination of hygroscopic molecules of water; however, these molecules are absorbed on the surface of $Mg(OH)_2$ particles. As a result, the adsorbing water molecules appear as a small endothermic starting at 48°C. The second thermal stage occurs at 353°C, which illustrates a loss of hydroxyl ions from the $Mg(OH)_2$ structure and varies into a distorted MgO structure. This stage demonstrates a crucial endothermic peak. A final stage with an exothermic peak was established at 375°C and referred to the initiating order cubic structure of MgO, which is compatible with the early experimental investigation [41-43].

4.2 XRD Analysis Technique

Generally, XRD can be used to characterize the crystallinity of nanoparticles. XRD patterns of the pure MgO-NPS and ($Mg_{(1.-x)}pb_xO$)-NPs specimens, where ($0 \leq x \leq 0.03$)after being calcinated at 420 °C, for 120 minutes with the rates of heating 3°C\min, are analyzed then compared with standard JCDPS cards.

The reflections are provided by the (Mg(1-x)pbxO)-NPs and pure MgO-.NPs specimens are seen in Figure 2. All specimens have Fm3m (#225) mostly as spacing category, and also, all doping specimens have the identical cubic structure to pure one [44].

The pure MgO-.NPs specimen, on the other side, demonstrated five significant peaks were observed at (36.6325, 42.6868, 61.9761, 74.3027, and 78.2192) that compatible with [ICSD PDF version 01-075-0447]. These conclusions are compatible with previous studies [24, 26, and 44].

The XRD Figure for the ($Mg_{0.97}Pb_{0.03}O$) specimen, on the other side, demonstrates an extra peak that correlates to the oxide of PbO. The unusual peaks occur at locations (29.20 and 30.315), respectively, that have been correlated with [ICSD PDF No. 00-005-0570] due to differences in ionic radius of Pb^{2+} and Mg^{2+}, which are (1.19 and 0.72) Å ions [44].

The mean size of crystallite (D) along the planes of (220) and (200) increased for the six samples located in the first part. In contrast, the diffracting factor of the ions of Pb^{2+} continued to increase due to facilitating the crystalline growth and crystallization of MgO-NPs. Furthermore, it can be attributed to the difference in ionic radius between dopants and host lattice; however, it was reduced for the ($Mg_{0.97}Pb_{0.03}O$) sample due to the formation of PbO Phase [44-46]. Figure 3 shows the variation of crystallite size according to the increase in the fraction of doping.

$$D = \frac{K\lambda}{\beta cos\theta} \quad (1)$$

4.3 FTIR Spectroscopy for (Mg(1.-x)pbxO)-NPs specimens

The Fourier transition infrared spectra of the produced ($Mg_{(1.-x)}pb_xO$)-NPs, ($0 \leq x \leq 0.03$) specimens by Pechini technique, calcianed at 420 °C for 120 minutes are demonstrated in Figure 4.

FT-IR for MgO-NPs specimen demonstrates that water molecules were adsorbed and absorbed on the surface of the specimen as cleared by the presence of broadband at (1650-3457) cm^{-1} allocated to the –OH bending and stretching vibrations, respectively, due to the special characteristic of MgO-NPs, in which it adsorbs moisture from the environment [47,48].

The vibrations of carbonate groups, however, the bands at the peak 1443 cm^{-1} corresponded to the vibrations of C-H. The absorption at the peaks 1250,1093,1050,860 cm^{-1} can be assigned to C-O vibration [28, 49, and 50]. Furthermore, due to atomic orbitals' vibrations, materials-based metal-oxide emit ranges between 1000 and 400 cm^{-1}.

For MgO-NPs specimens, the area correlates to Mg-O about 782-400 cm^{-1}, which correlates to Mg-O or Mg-O-Mg deformation vibration [51].

A comparison of the doping specimens demonstrates that all spectra have identical signals since they all comprise the same key framework part, the MgO-NPs structures [52, 53] nearly slight variation in the band's intensity in 3450-1650 cm^{-1}. This can be attributed to -OH stretching frequency assigned due to the hydroxyl group present in the oxide [47, 54]. There was a slight shift in the carbonate groups band due to the incorporation of more binding Pb molecular in the ranging 1650-805 cm^{-1}. However, there is notable variation in the intensity of the C-H bands with increasing the fraction of doping [54]. The bands at about 804-400 cm^{-1} are assigned to O-Mg [55] and O-Pb [56] vibrations, respectively. It can be noted that the bands get broader, and the intensities increase as the incorporation of Pb^{2+} ions increases in the ranging 800-400 cm^{-1} due to the difference in the electronic structure between Pb^{2+} and MgO host lattice [57].

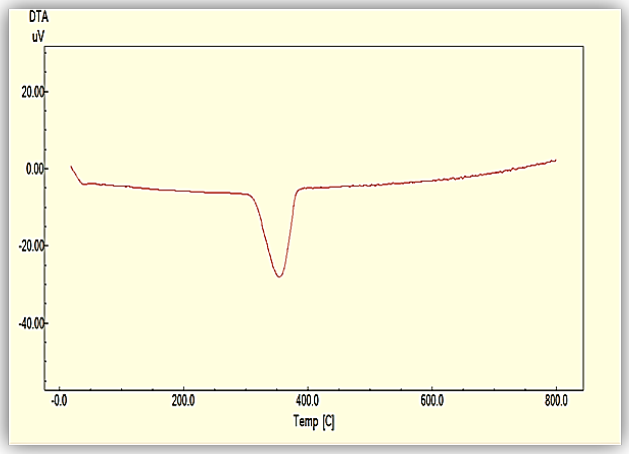

$$Mg(OH)_2 \xrightarrow{decomposition} MgO + H_2O$$

Figure 1: DTA curve of $Mg(OH)_2$ decomposition thermally in the ithe temperature ranging from 25 - 800 °C with the rates of heating 10 °C\.min-1

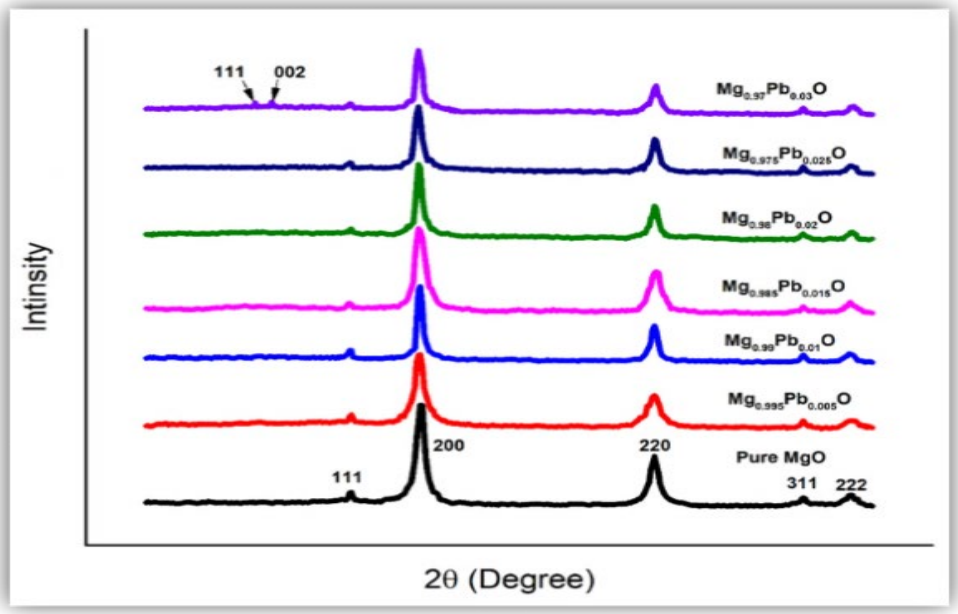

Figure 2: XRD analysis for (Mg1-xpbxO)-NPs specimens calcined at 420oC for 120 minutes [44]

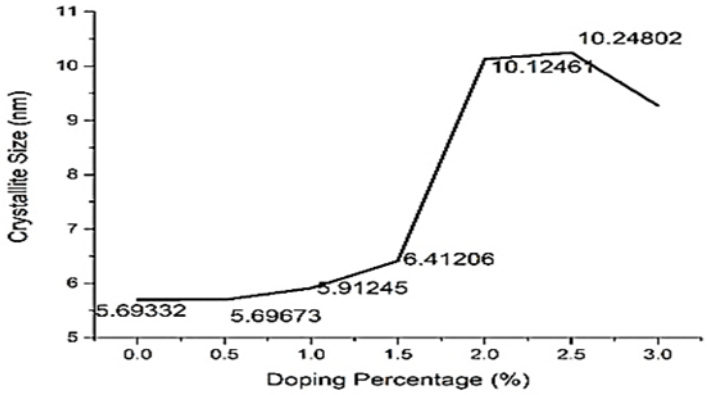

Figure 3: The relationship between crystalline size and increasing in the percentage of doping

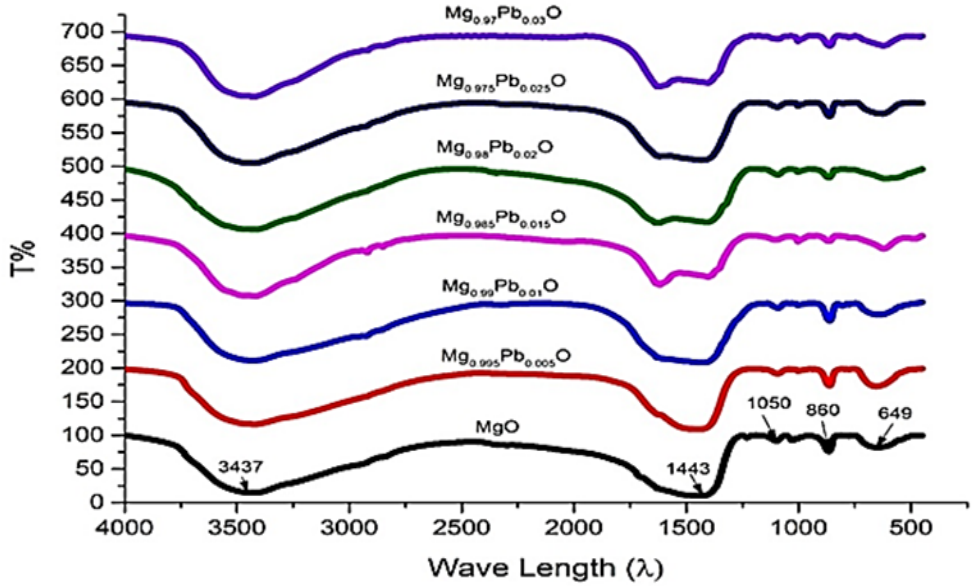

Figure 4: FTIR for Mg(x-1)PbxO specimens calcined at 420oC for 120 minutes

5. Conclusions

All the doped and pure specimens were successfully made by the modified Pechini procedure. The temperature of decomposition thermally from $Mg(OH)_2$ to MgO was 375°C. The structure investigation revealed that all the specimens have identical space groups and index well to cubic structure. The obtained crystallite size by Scherrer's equation was increased with increasing the fraction of doping except for ($Mg_{0.97}Pb_{0.03}O$) due to the formation of PbO oxide. The molecular vibration demonstrated that all the pure and doped specimens have the same framework. As the incorporation of Pb^{2+} ions increased, the bands got broader. The intensities increased in the ranging 800-400 cm^{-1} confirmed the incorporation of Pb^{2+} ions into the place of Mg^{2+} ions in the lattice.

Author contribution

All authors contributed equally to this work.

Funding

This research received no specific grant from any funding agency in the public, commercial, or not-for-profit sectors.

Data availability statement

The data that support the findings of this study are available on request from the corresponding author.

Conflicts of interest

The authors declare that there is no conflict of interest.

References

[1] H. Greim, Constitution and procedures of the commission for the investigation of health hazards of chemical compounds in the work area, WILEY, Germany, Report 52 (2016).

[2] W. Z. Lin. Characterization of nanophase materials, Wiley-VCH, 1st ed, Germany, (2000).

[3] T. Iqbal, S. Tufail, and S. Ghazal, Synthesis of silver, chromium, manganese, tin and iron nano particles by different techniques, Int. J. Nanosci. Nanotechnol., 13 (2017) 19–52.

[4] T. I. Shabatina, O. I. Vernaya, V. P. Shabatin, and M. Y. Melnikov, Magnetic nanoparticles for biomedical purposes: modern trends and prospects, Magnetochemistry., 6 (2020). https://doi.org/10.3390/magnetochemistry6030030

[5] S. Thomas, B. S. P. Harshita, P. Mishra, and S. Talegaonkar, Ceramic nanoparticles: fabrication methods and applications in drug delivery, Curr. Pharm. Des., 21 (2015) 6165–6188. https://doi.org/10.2174/1381612821666151027153246

[6] A. Tarutin, N. Danilov, J. Lyagaeva, and D. Medvedev, One-step fabrication of protonic ceramic fuel cells using a convenient tape calendering method, Appl. Sci., 10 (2020). https://doi.org/10.3390/app10072481

[7] S. Wang and L. Gao. Laser-driven nanomaterials and laser-enabled nanofabrication for industrial applications, Ind. Appl. Nanomater., Elsevier, (2019) 181-203. https://doi.org/10.1016/B978-0-12-815749-7.00007-4

[8] C. Wang, Z. hai Shi, L. Peng, W. min He, B. liang Li, and K. zhi Li, Preparation of carbon foam-loaded nano-TiO_2 photocatalyst and its degradation on methyl orange, Surf. Interfaces., 7 (2017) 116–124. https://doi.org/10.1016/j.surfin.2017.03.007

[9] K. Harun, N. Mansor, Z. A. Ahmad, and A. A. Mohamad, Electronic properties of zno nanoparticles synthesized by sol-gel method: a lda+u calculation and experimental study, Procedia Chem., 19 (2016) 125–132. https://doi.org/10.1016/j.proche.2016.03.125

[10] S. Tumanski, Handbook of magnetic measurements, CRC press, Series in Sensors, USA (2011). https://doi.org/10.1201/b10979

[11] Z. X. Tang and B. F. Lv, MgO nanoparticles as antibacterial agent: Preparation and activity, Brazilian J. Chem. Eng., 31 (2014) 591–601. https://doi.org/10.1590/0104-6632.20140313s00002813

[12] N. A. Hamid, N. F. Shamsudin, and K. W. Seec, Superconducting properties and mechanical strength of MgO fibres reinforced bulk Bi-2212 superconductor ceramics, Mater. Res. Innov., 13 (2009) 379–381. https://dx.doi.org/10.1179/143307509x441612

[13] Z. X. Tang, X. J. Fang, Z. L. Zhang, T. Zhou, X. Y. Zhang, and L. E. Shi, Nanosize MgO as antibacterial agent: Preparation and characteristics, Brazilian J. Chem. Eng., 29 (2012) 775–781. https://doi.org/10.1590/S0104-66322012000400009

[14] A. Dahmardeh and A. M. Davarpanah, Short communication investigation on influences of synthesis methods on the magnetic properties of trimetallic nanoparticles of iron-cobalt- manganese supported by magnesium oxide, Int. J. Nanosci. Nanotechnol.,11 (2015) 249–256.

[15] T. Thangeeswari, M. Priya, and J. Velmurugan, Enhancement in the optical and magnetic properties of ZnO:Co implanted by Gd3+ nanoparticles, J. Mater. Sci. Mater. Electron., 26 (2015) 2436–2444. https://doi.org/10.1007/s10854-015-2703-2

[16] O. Elimelech, J. Liu, A. M. Plonka, A. I. Frenkel, and U. Banin, Size dependence of doping by a vacancy formation reaction in copper sulfide nanocrystals, Angew. Chemie., 129 (2017) 10471–10476. https://doi.org/10.1002/ange.201702673

[17] R. John and R. Rajakumari, Synthesis and characterization of rare earth ion doped nano ZnO, Nano-Micro Lett., 4 (2012) 65–72. https://doi.org/10.1007/BF03353694

[18] D. Misra and S. K. Yadav, Prediction of site preference of implanted transition metal dopants in rock-salt oxides, Sci. Rep., 9 (2019). https://doi.org/10.1038/s41598-019-49011-5

[19] S. C. Erwin, L. Zu, M. I. Haftel, A. L. Efros, T. A. Kennedy, and D. J. Norris, Doping semiconductor nanocrystals, Nature, 436 (2005) 91–94. https://doi.org/10.1038/nature03832

[20] U. Sharma and P. Jeevanandam, Synthesis of Zn2+-doped MgO nanoparticles using substituted brucite precursors and studies on their optical properties, J. Sol-Gel Sci. Technol., 75 (2015) 635–648. https://doi.org/10.1007/s10971-015-3734-0

[21] V. Vasanthi, M. Kottaisamy, K. Anitha, and V. Ramakrishnan, Near UV excitable yellow light emitting Zn doped MgO for WLED application, Superlattices Microstruct., 106 (2017) 174–183. https://doi.org/10.1016/j.spmi.2017.03.050

[22] U. Sharma and P. Jeevanandam, Layered double hydroxides as precursors to Ti4+ doped MgO nanoparticles with tunable band gap, J. Nanosci. Nanotechnol., 18 (2018) 264–278. https://doi.org/10.1166/jnn.2018.14557

[23] J. W. Lee and J. H. Ko, Defect states of transition metal-doped MgO for secondary electron emission of plasma display panel, J. Inf. Disp., 15 (2014) 157–161. https://doi.org/10.1080/15980316.2014.955140

[24] S. Azzaza, M. El-Hilo, S. Narayanan, J. Judith Vijaya, N. Mamouni, A. Benyoussef, A. El Kenz, and M. Bououdina. Structural, optical and magnetic characterizations of Mn-doped MgO nanoparticles, Mater. Chem. Phys., 143(2014) 1500-1507. https://doi.org/10.1016/j.matchemphys.2013.12.006

[25] G. T. Fox, M. W. Wolfmeyer, J. R. Dillinger, and D. L. Huber, Magnetic field dependence of the thermal conductivity of doped MgO, Phys. Rev., 165 (1968) 898–901. https://doi.org/10.1103/PhysRev.165.898

[26] C. Yuncheng, D. Wu, X. Zhu, W. Wang, F. Tan, J. Chen, X. Qiao, and X.O. Qiu. Sol-gel preparation of Ag-doped MgO nanoparticles with high efficiency for bacterial inactivation, Ceram. Int., 43 (2017) 1066-1072. https://doi.org/10.1016/j.ceramint.2016.10.041

[27] U. Sharma and P. Jeevanandam, Synthesis of Zn2+-doped MgO nanoparticles using substituted brucite precursors and studies on their optical properties, J. Sol-Gel Sci. Technol., 75 (2015) 635–648. https://doi.org/10.1007/s10971-015-3734-0

[28] B. Kim and H. Lee, Valence state and ionic conduction in Mn-doped MgO partially stabilized zirconia, J. Am. Ceram. Soc., 101 (2018) 1790–1795. https://doi.org/10.1111/jace.15333

[29] L. Peng, Y. Wang, Z. Wang, and Q. Dong, Multiplesite structure and photoluminescence properties of Eu3+ doped MgO nanocrystals, Appl. Phys. A Mater. Sci. Process., 102 (2011) 387–392. https://doi.org/10.1007/s00339-010-6027-z

[30] M. Sadeghi, and M. Hosseini. Nucleophilic chemistry of the synthesized magnesium oxide (magnesia) nanoparticles via microwave sol-gel process for removal of sulfurous pollutant, Int. J. Bio-Inorg. Hybr. Nanomater.,1 (2012) 175-182.

[31] B. Zaidi, S. Belghit, M. S. Ullah, B. Hadjoudja, A. Guerraoui, S. Gagui, N. Houaidji, B. Chouial, and C. Shekhar, Investigation of MgO powders synthesized by liquid-phase method, Metallofiz. Noveishie Tekhnol., 41 (2019) 1121-1126. https://doi.org/10.15407/mfint.41.08.1121

[32] K. Ganapathi Rao, C. Ashok, K. Venkateswara Rao, and C. Shilpa Chakra, Structural properties of MgO nanoparticles: synthesized by co-precipitation technique, Int. J. Sci. Res., (2013) 43–46.

[33] M. Y. Nassar, T. Y. Mohamed, I. S. Ahmed, and I. Samir, MgO nanostructure via a sol-gel combustion synthesis method using different fuels: An efficient nano-adsorbent for the removal of some anionic textile dyes, J. Mol. Liq., 225 (2017) 730–740. https://doi.org/10.1016/j.molliq.2016.10.135

[34] M. R. Mohammad Shafiee, M. Kargar, and M. Ghashang, Characterization and low-cost, green synthesis of Zn2+ doped MgO nanoparticles, Green Process. Synth.,7 (2018) 248–254. https://doi.org/10.1515/gps-2016-0219

[35] W. C. Li, A. H. Lu, C. Weidenthaler, and F. Schüth, Hard-templating pathway to create mesoporous magnesium oxide, Chem. Mater., 16 (2004) 5676–5681. https://doi.org/10.1021/cm048759n

[36] P. Jeevanandam and K. J. Klabunde, A study on adsorption of surfactant molecules on magnesium oxide nanocrystals prepared by an aerogel route, Langmuir., 18 (2002) 5309–5313. https://doi.org/10.1021/la0200921

[37] C. Y. Tai, C. Te Tai, M. H. Chang, and H. S. Liu, Synthesis of magnesium hydroxide and oxide nanoparticles using a spinning disk reactor, Ind. Eng. Chem. Res., 46 (2007) 5536–5541. https://doi.org/10.1021/ie060869b

[38] S. Ghorbani, R. S. Razavi, M. R. Loghman-Estarki, and A. Alhaji, Development of $MgO–Y_2O_3$ composite nanopowder by pechini Sol–Gel method: effect of synthesis parameters on morphology, particle size, and phase distribution, J. Clust. Sci., 28 (2017) 1523–1539. https://doi.org/10.1007/s10876-017-1162-8

[39] M. P. Pechini, Method of preparing lead and alkaline earth titanates and niobates and coating method using the same to form a capacitor, US Patent No. 3330697, (1967).

[40] M. A. Zalapa-Garibay, A. Arizmendi-Moraquecho, and S. Y. Reyes-López, Low temperature synthesis of alpha alumina platelets and acicular mullite in $MgO\text{-}Al_2O_3\text{-}SiO_2$ system, J. Ceram. Sci. Technol., 10 (2019) 9–18. http://dx.doi.org/10.4416/JCST2018-00043

[41] V. Karthikeyan, S. Dhanapandian, and C. Manoharan, Characterization and antibacterial behavior of MgO-PEG nanoparticles synthesized via co-precipitation method, Int. Lett. Chem. Phys. Astron., 70 (2016) 33–41.http://dx.doi.org/10.18052/www.scipress.com/ILCPA.70.33

[42] H. Dong, C. Unluer, E. H. Yang, and A. Al-Tabbaa, Recovery of reactive MgO from reject brine via the addition of NaOH, Desalination, 429 (2018) 88–95. https://doi.org/10.1016/j.desal.2017.12.021

[43] K. G. Rao, C. H. Ashok, K. V. Rao, and C. H. S. Chakra, Structural properties of MgO nanoparticles : synthesized by co-precipitation technique, December (2015).

[44] I. A. Najem, S. J. Edrees, and F. A. Rasin. Structural and magnetic characterisations of Pb-doped MgO nanoparticles by a modified pechini method, IOP Conf. Ser.: Mater. Sci. Eng. 987, 2020, 012027. https://doi.org/10.1088/1757-899x/987/1/012027

[45] A. Ansari, A. Ali, M. Asif, and Shamsuzzaman, Microwave-assisted MgO NP catalyzed one-pot multicomponent synthesis of polysubstituted steroidal pyridines, New J. Chem., 42 (2018) 184–197. https://doi.org/10.1039/C7NJ03742B

[46] A. Das, A. C. Mandal, S. Roy, and P. M. G. Nambissan, Internal defect structure of calcium doped magnesium oxide nanoparticles studied by positron annihilation spectroscopy, AIP Adv., 8 (2018). https://doi.org/10.1063/1.5001105

[47] H. Cui, X. Wu, D. Zhang, J. Zhang, H. Xiao, and Y. Chen, Thermotolerance and antibacterial properties of MgO-triclosan nanocomposites, Procedia Eng., 102 (2015) 410–416. https://doi.org/10.1016/j.proeng.2015.01.175

[48] A. Ansari, A. Ali, M. Asif, and Shamsuzzaman, Microwave-assisted MgO NP catalyzed one-pot multicomponent synthesis of polysubstituted steroidal pyridines, New J. Chem., 42 (2018) 184–197. https://doi.org/10.1039/C7NJ03742B

[49] W. C. Wee, Y. S. Chan, J. Jeevanandam, K. Pal, M. Bechelany, M. Abd Elkodous, and G. S. El-Sayyad, Response surface methodology optimization of mono-dispersed MgO nanoparticles fabricated by ultrasonic-assisted sol–gel method for outstanding antimicrobial and antibiofilm activities, J. Cluster Sci.,31 (2020) 367-389. https://doi.org/10.1007/s10876-019-01651-3

[50] S. Manikandan and K. S. Rajan, Rapid synthesis of MgO nanoparticles & their utilization for formulation of a propylene glycol based nanofluid with superior transport properties, RSC Adv., 4 (2014) 51830–51837. https://doi.org/10.1039/C4RA09173F

[51] R. Dobrucka, Synthesis of MgO nanoparticles using artemisia abrotanum herba extract and their antioxidant and photocatalytic properties, Iran. J. Sci. Technol. Trans. A Sci., 42 (2018) 547–555. https://doi.org/10.1007/s40995-016-0076-x

[52] S. Yousefi and B. Ghasemi, Precipitator concentration-dependent opto-structural properties of MgO nanoparticles fabricated using natural brine, SN Appl. Sci., 2 (2020). https://doi.org/10.1007/s42452-020-2645-z

[53] N. C. S. Selvam, R. T. Kumar, L. J. Kennedy, and J. J. Vijaya, Comparative study of microwave and conventional methods for the preparation and optical properties of novel MgO-micro and nano-structures, J. Alloys Compd., 509 (2011) 9809–9815. https://doi.org/10.1016/j.jallcom.2011.08.032

[54] J. L. Boldu, E. Muñoz, O. Novaro, T. Lopez, and R. Gomez, Crystalline structure and morphology of the phases in MgO, TiO_2 and ZrO_2 prepared by the sol-gel technique, MRS Online Proceedings Library (OPL) 405, (1995). https://doi.org/10.1557/PROC-405-523

[55] N. Jamil, M. Mehmood, A. Lateef, R. Nazir, and N. Ahsan, MgO nanoparticles for the removal of reactive dyes from wastewater, TechConnect Briefs.,1 (2015) 353–356.

[56] S. Elawam, W. Morsi, H. Abou-Shady, and O. Guirguis, Characterizations of beta-lead oxide 'massicot' nano-particles, Curr. Appl. Sci. Technol., 17 (2016) 1–10. http://dx.doi.org/10.9734/BJAST/2016/28143

[57] G. M. Montserrat, Synthesis and characterization of optical nanocrystals and nanostructures. An approach to transparent laser nanoceramics, PhD Thesis, Universitat Rovirai i Virgili, Tarragona，2011.